Article

Not peer-reviewed version

Synthesis, Characterisation, Biological Evaluation and In Silico Studies of Quinoline-1,2, 3-Triazole-Anilines as Potential Antitubercular and Anti-HIV Agents

Snethemba S. Magwaza , Darian Naidu , Oluwatoba E Oyeneyin , Sibusiso Senzani , Nompumelelo P Mkhwanazi , Matshawandile Tukulula *

Posted Date: 11 April 2025

doi: 10.20944/preprints202504.0967.v1

Keywords: quinoline-1,2,3-triazole-anilines; click reaction; HIV-1 subtype B; molecular docking; density functional theory

 doi:10.20944/preprints202504.0967.v1

Article

Synthesis, Characterisation, Biological Evaluation and *In Silico* Studies of Quinoline-1,2,3-triazole-anilines as Potential Antitubercular and Anti-HIV Agents

Snethemba S. Magwaza [1], Darian Naidu [2], Oluwatoba E. Oyeneyin [1,3], Sibusiso Senzani [4], Nompumelelo P. Mkhwanazi [2] and Matshawandile Tukulula [1,*]

[1] School of Chemistry and Physics, University of KwaZulu Natal, Westville Campus, Durban, 4001, South Africa; TukululaM@ukzn.ac.za; MagwazaS@ukzn.ac.za

[2] HIV Pathogenesis Programme, Doris Duke Medical Research Institute, School of Laboratory Medicine and Medical Sciences, College of Health Sciences, University of KwaZulu Natal, Durban, 4001, South Africa; Mkhwanazi@ukzn.ac.za; 218052764@stu.ukzn.ac.za

[3] Department of Chemical Sciences, Adekunle Ajasin University, Akungba-Akoko, Ondo State, Nigeria; Oyeneyin.oluwatoba@aaua.edu.ng

[4] School of Laboratory Medicine and Medical Sciences, College of Health Sciences, University of KwaZulu Natal, Durban, 4001, South Africa; SenzaniS@ukzn.ac.za

* Correspondence: tukululam@ukzn.ac.za; Tel.: +27-31-260-8756; Fax: +27-31-260-3091

Abstract: HIV/AIDS and *Mycobacterial tuberculosis* (*Mtb*) are the leading cause of deaths worldwide. Thus, better medicaments are required to manage these diseases. Quinolines have shown great potential due to their broad spectrum of biological activity. Thus, quinoline-1,2,3-triazole-aniline hybrids were synthesised in moderate to good yields. Compounds **11g** (IC_{50} = 0.388 μM), **11h** (IC_{50} = 0.01032 μM) and **11i** (IC_{50} = 0.167 μM) exhibited the most promising *in vitro* activities against the wild-type HIV-1 subtype B, with **11h** being 9-fold more active than AZT (IC_{50} = 0.0909 μM), the reference drug. Furthermore, compound **11h** displayed moderate activity with MIC_{90} of 88μM against *Mtb*'s H37Rv strain. Cytotoxicity studies on TZM-bl-cell lines revealed that most of the tested compounds were generally non-cytotoxic; the selectivity index (SI) for **11h**, the front runner, is > 2472. Molecular docking studies revealed that **11h** interacted with Phe112, Tyr108, Glu283, and Trp86 amino acid residues in the active site of the HIV-1. DFT studies revealed that **11h** has the ability to donate and accept electrons to and from available orbitals. The predicted ADMET studies showed that these compounds possess drug-likeness, and **11h** has the potential to be further optimisation as anti-HIV-1 agent.

Keywords: Quinoline-1,2,3-triazole-anilines; click reaction; HIV-1 subtype B; molecular docking; and density functional theory

1. Introduction

Africa and other developing countries have borne a substantial burden of mortality attributed to infectious diseases [1,2]. One of the most concerning infectious diseases, Tuberculosis (TB), is caused by *Mycobacterium tuberculosis* (*Mtb*), a gram-negative bacterium with a lipid-rich outer membrane that makes it resilient against various antibiotics [3–5]. To treat drug-susceptible TB, combinations of isoniazid, rifampicin, pyrazinamide, and ethambutol, termed first-line drugs, are administered [6–8]. Each of these drugs targets specific areas in *Mtb* with the shared objective of inhibiting the production of essential biological processes critical for bacterial replication and survival [6]. Over the years, due to the gene mutations, *Mtb* has evolved to more resistant isoforms,

 doi:10.20944/preprints202504.0967.v1

such as multi-drug resistant (MDR-TB), extensively drug-resistant (XDR-TB) and totally drug-resistant TB (TDR-TB) [9,10].

On the other hand, the human immunodeficiency virus (HIV) remains one of the most prevalent infectious diseases [11]. To date, 39.9 million people are living with HIV/AIDS (PLWH) worldwide [12]. Effective drug development over the years has saved many lives, with the discovery of the Highly active antiretroviral therapy (HAART) being the pivotal moment. The use of antiretroviral drugs has decreased the morbidity and mortality rate of PLWH by turning HIV-1 into a chronic and manageable disease [13,14]. Despite HAART's early success, drug-resistant mutant development rendered it less effective over time. HIV is a complex virus with a high mutation rate, considering it replicates in several replication stages. Antiretroviral drugs target different stages of the HIV-1 life cycle: viral attachment, reverse transcription, integration, proteolysis and viral budding [15]. There are seven classes of antiretrovirals based on their molecular mechanisms and resistance profiles, namely: nucleoside-analogue reverse transcriptase inhibitors (NNRTIs), non–nucleoside reverse transcriptase inhibitors (NNRTIs), integrase inhibitors, protease inhibitors (PIs), fusion inhibitors, post-attachment inhibitor (PAI) and co-receptor antagonists [16–19]. These drug regimens constantly evolve, and new drugs are continually being developed in each class.

Various quinoline- and/or 1,2,3-triazole-containing compounds have been reported to show promising activities against either *Mtb* [20–28] or HIV infections [29–32], with some already in clinical settings, including the 1,2,3 triazole-pyrimidine hybrids that are now part of the second generation NNRTI's [30]. Bedaquiline (or TMC-207) (**Figure 1**), a quinoline-based compound, is clinically utilised for treating multidrug-resistant TB [33]. This compound binds to the subunit C of mycobacterial ATP synthase, an essential enzyme for *Mtb* energy production and survival. However, bedaquiline suffers from several side effects due to its potent inhibition of the potassium ether-ago-go-related gene (hERG) that could potentially lead to cardiac arrest [34]. Thus, new quinoline-based anti-*Mtb* agents, devoid of bedaquiline's shortcomings, are critically important. Due to the broad spectrum of activities, various quinoline-triazole hybrids have shown promise over the years. Thomas *et al.* [21] reported on a series of new 6-methoxyquinoline triazole amides (**1**) (MIC = 0.625 μg/ml), sulphonamides (**2**) (MIC = 0.625 μg/ml), and amidopiperazines (**3**) (MIC = 0.625 μg/ml) that exhibited promising antitubercular activities. Our group recently disclosed a series of 7-chloroquinoline-triazole-benzimidazole hybrids that demonstrated excellent *Mtb* activity, with isomeric mixture **4** showing MIC_{90} of 1.49 μM [22]. Previously, Costa *et al.* [29] reported several quinoline-1,2,3-triazole hybrids, such as **5** (IC_{50} = 800 nm), that showed promising activity against HIV reverse transcriptase. Maraviroc, the first licensed CCR5 co-receptor antagonist containing the triazole moiety, is used to treat HIV infections and is less prone to drug resistance than the presently used ([N]NRTI) [35–37].

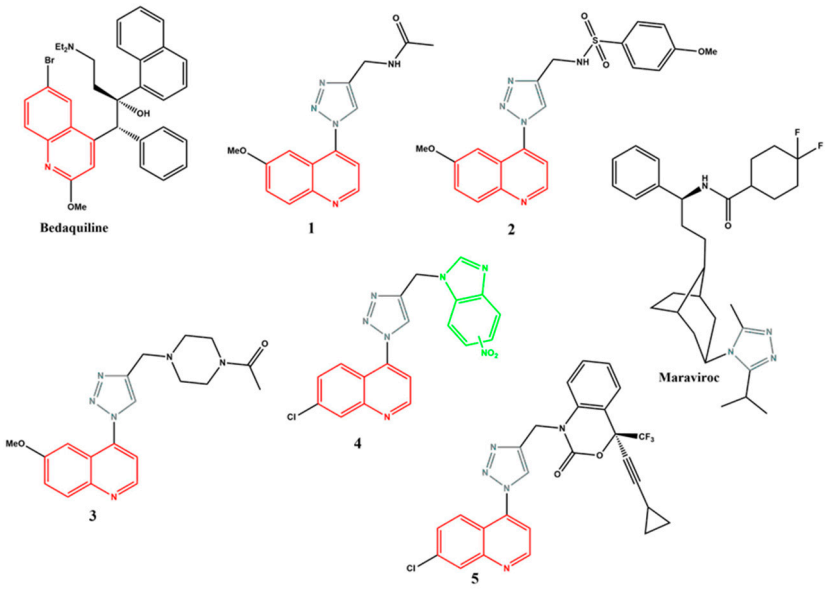

 doi:10.20944/preprints202504.0967.v1

Figure 1. Quinoline and triazole-containing compounds that show antitubercular and antiviral activity.

Simultaneously targeting TB and HIV is of paramount importance, especially considering the high prevalence of co-infection, drug resistance and the potential for drug-drug interactions in patients receiving treatment for both diseases [38]. Combining quinoline and triazole scaffolds into hybrid structures may synergistically improve efficacy against both *Mtb* and HIV [39,40]. The structural analysis of some of the compounds shown in Figure 1 reveals common structural features, shown in blue in **Figure 2**. Could these structural features be responsible for these compounds combined anti-*Mtb* and anti-HIV activities? Thus, in this study, we report on the synthesis, biological evaluation and computational studies of a series of compounds containing these structural features, albeit with the substitution of the quinoline moiety limited to the 7-chloro only.

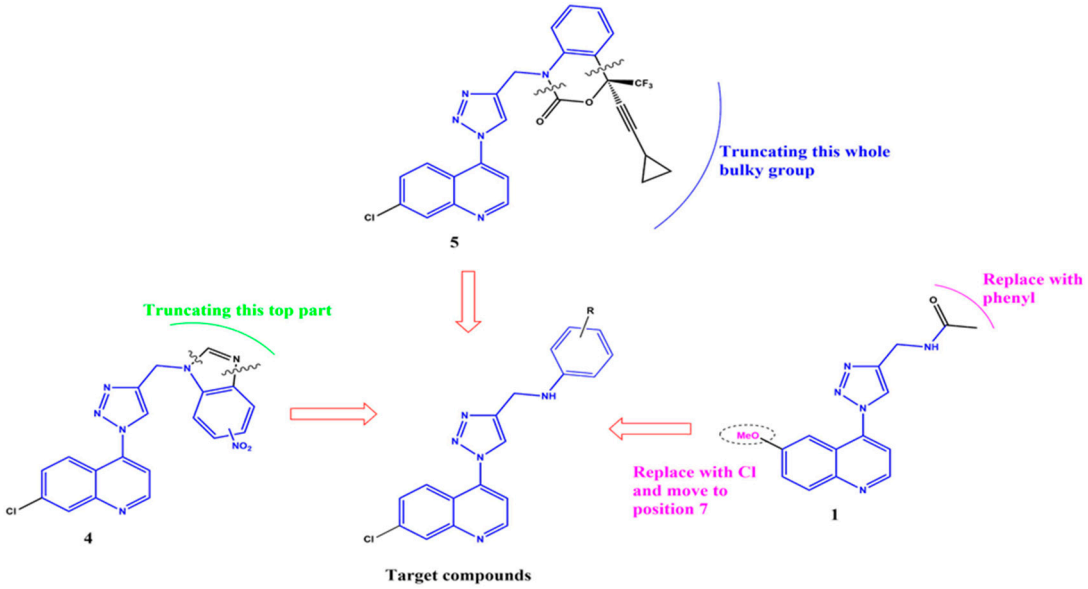

Figure 2. Rationale for the target compounds.

2. Results and Discussion

2.1. Chemistry

The target compounds were synthesised in two stages, as shown in **Scheme 1**. The first stage is the formation of the two key intermediates, namely the 7-chloroquinoline-4-azide **7** and the alkyne **10a-j**, *via* steps 1 and 2. These intermediates are then subjected to "Click chemistry" [27] in step 3 to yield the final quinoline-1,2,3, triazole-aniline derivatives, **11a-j**, in 43 to 92% yields (**Table 1**). 1D and 2D nuclear magnetic resonance (NMR) and infrared (IR) spectroscopy were used to confirm the structures, while mass spectrometry confirmed the masses of the desired products (*see supplementary information*).

Confirmation of the 1,2,3-triazole formation was achieved by observing the chemical shift of the singlet triazole methine proton, which appears in the aromatic region around δ_H 8.7 ppm. Secondly, the methylene doublet, due to coupling with the neighbouring NH, appears as expected at around 4.47 ppm, while the NH appears as a triplet at 6.21 ppm. All the quinoline protons are appearing as expected. The ^{13}C NMR ATP NMR analysis also confirmed the formation of the hybrid, with the critical methine and methylene resonances appearing at 125.68 and 38.95 ppm, respectively.

Preprints.org (www.preprints.org) | NOT PEER-REVIEWED | Posted: 11 April 2025 doi:10.20944/preprints202504.0967.v1

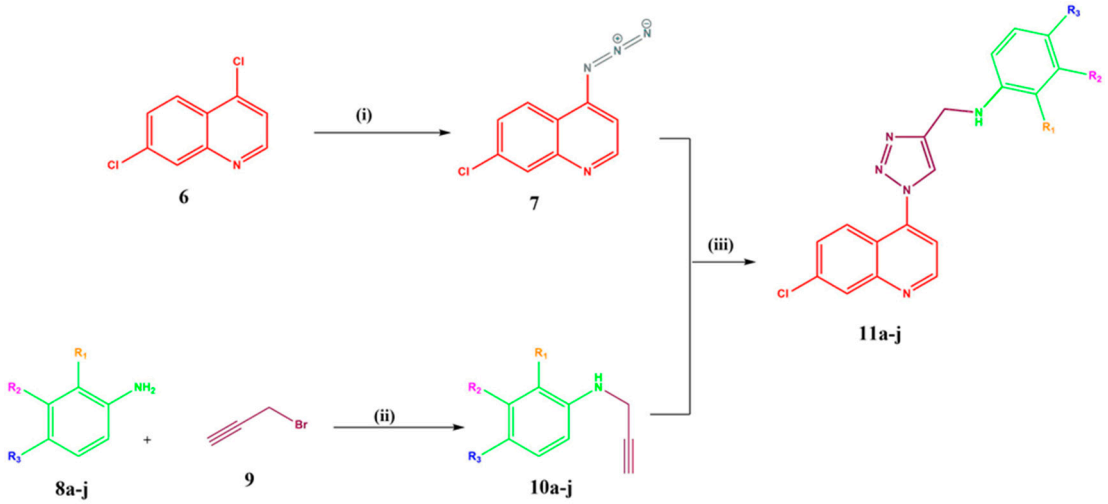

Scheme 1. Synthesis of the target compounds 11a-j. Reagents and conditions: (i) NaN_3, DMF, 85 °C, 24 hrs; (ii) K_2CO_3, DCM, rt, 24 hrs; (iii) sodium ascorbate, $CuSO_4$, DCM, 24 hrs.

Table 1. Yields, melting points and masses of the target compounds.

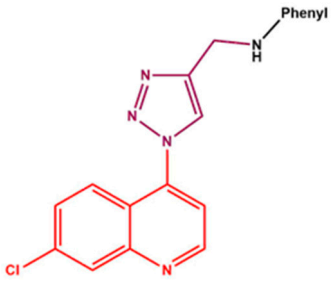

Compound	Phenyl	Appearance	% Yield	m.p. (°C)	MS data
11a	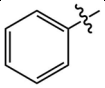	cream white solid	88	150-152	306.0968 $[(M-H)-N_2]^-$
11b	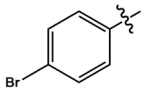	light brown solid	87	188-190	449.9707 $[(M+HCl]^-$
11c	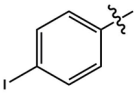	brown solid	92	198-199	495.9821 $[(M-H)+Cl]^-$
11d	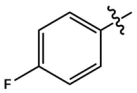	light grey solid	79	145-147	324.0866 $[(M-H)-N_2]^-$
11e	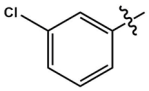	Yellow solid	69	169-171	340.0580 $[(M-H)-N_2)]^-$
11f	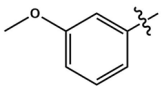	dark brown liquid	43	-	388.1096 $(M+Na)^+$

 doi:10.20944/preprints202504.0967.v1

11g	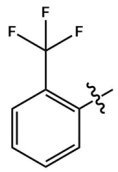	Yellow liquid	48	-	-
11h	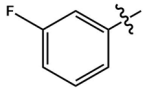	cream white solid	85	145-147	324.0868 $[(M-H)-N_2]^-$
11i	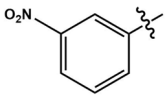	Orange solid	79	192-194	381.2533 $(M+1)^-$
11j	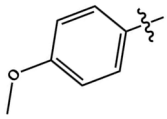	Brown solid	86	169-172	336.1097 $[(M-H)-N_2]^-$

The heteronuclear multiple bond correlations (HMBC) experiment (**Figure 3**) further validated the triazole ring formation, with close correlations of H6-C13, H1-C13, H1-C6 and H6-C14 being observed and shown in the structure of **11a**. The mass spectrometry confirmed the masses of the target compounds based on their main or major fragment as observed in the base peak. All the other compounds were characterized in a similar manner.

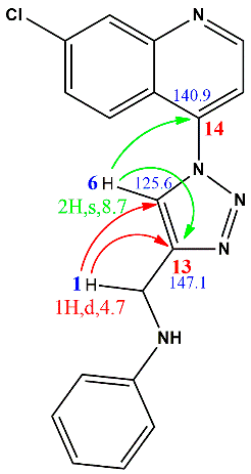

Figure 3. HMBC spectrum in DMSO-d6 and illustration of vital HMBC correlation in compound **11a**.

2.2. In Vitro Biological Activities

The synthesised quinoline-1,2,3-triazole anilines were evaluated in vitro against *Mtb* H37Rv (ATCC 27294) strain, against HIV-1 subtype B, and their cytotoxicity assessed using MTT assay on TZM-bl cell-line (**Table 2**). The *Mtb* activity is represented as the 90% minimum inhibitory concentration (MIC_{90}), while HIV and cytotoxicity are represented as the 50% inhibitory concentration (IC_{50}) and 50% cytotoxicity concentration (CC_{50}), respectively. In terms of anti-*Mtb*, the data reveals that all the synthesised hybrid compounds did not show any appreciable activity, with compounds **11b**, **11c**, **11i** and **11j** exhibiting poor activity (MIC_{90} > 1000 μM), while **11a**, **11d-g**, and 11i fell within the range of 100-200 μM. Notably, compound **11h** exhibited the most potent activity with MIC_{90} of 88μM, distinguishing it as the most active among all these, albeit 9-fold less active than the reference drug, ethambutol.

 doi:10.20944/preprints202504.0967.v1

Against HIV-1, initially, all the compounds showed > 50% inhibition in primary inhibition assay were progressed to determine their IC_{50}, and azidothymidine (AZT) was used as a control drug. Generally, all the compounds inhibited the growth of the HIV-1 subtype B virus, ranging from 58-100% inhibition potential (*see percentage cell viability plots in the supplementary information*). The IC_{50} values for most of these compounds were moderate, with only three compounds exhibiting sub-micromolar activity, namely **11g**, **11h** and **11i**, albeit not as active as AZT. Compound **11g** (consisting of the trifluoromethyl substituent on the phenyl ring) (IC50 = 0.3883 μM) and **11i** (the 3-nitrosubstituted) (IC_{50} = 0.170 μM) were 4- and 1.8-fold less active than AZT, respectively. On the other hand, **11h** (the 3-flourosubstituted) (IC_{50} = 0.01032 μM) is 8.8 times more potent than AZT. Interestingly, compound 11h was also the most active against Mtb, highlighting its dual active potential. Cytotoxicity assessment revealed that five of the synthesised compounds, **11a**, **11c-e** and **11g**, exhibited CC_{50} >100 μM, with 11g showing the best cytotoxicity profile with CC_{50} = 4414 μM and selectivity index (SI) of > 11300, which is not far off from that of AZT (SI = 12349). On the other hand, the CC_{50} value of compound **11h** was 25.52 μM and its SI > 2400, an indication of the less likely to be cytotoxic in vivo [41,42]. Thus, compound **11h** is a potential "hit" compound for further optimisation as a potential anti-HIV agent based on its activity and cytotoxicity profile.

Table 2. Anti-*Mtb*, -HIV and cytotoxicity evaluation of quinoline 1,2,3-triazole-anilines.

Compound	Anti-*Mtb* (μM)	Anti-HIV (μM)	Cytotoxicity CC_{50} (μM)	SI[a]
	$H_{37}Rv$ MIC_{90}	HIV-1 Subtype B IC_{50}	TZM-bl cell line	(CC_{50}/IC_{50})
11a	186.52	3.013	177.1	58.75
11b	1210.65	124.4	0.248	1.994 x 10-3
11c	1084.6	23.20	156.9	6.76
11d	176.52	DNC*	1320.0	-
11e	168.81	713.7	834.6	1.17
11f	171.19	22.75	3.599	0.158
11g	155.05	0.3883	4414	11367.49
11h	88.72	0.01032	25.52	2472.87
11i	nd*	0.167	0.00901	0.05
11j	1369.86	180.4	4.000	0.02
7	19.09	nd*	nd*	-
10a	3814	nd*	nd*	-
Ethambutol	9.68	-	-	-
AZT	-	0.0909	1122.58	12349.59

[a]SI: Selectivity index; *DNC: Did not converge to give IC_{50} values; [#]nd: not determined;.

2.3. In Silico Studies

2.3.1. Molecular Docking

To validate the observed biological activities, all hybrid compounds underwent *in silico* docking simulations into the active site of the *Mtb* ATP synthase enzyme (PDB ID: 4VIF) [43] and the antiviral enzyme (PDB ID: 4MBS) [44] using the Maestro software in Schrödinger Suite [45]. Docking scores recorded in **Table 3** ranged from -2.879 to -2.035 kcal/mol for the antimicrobial target and -7.371 to -4.815 kcal/mol for the antiviral target. Compound **11d** had the best docking score, followed by **11e** and **11h** against the antiviral enzyme, while **11e** had the best docking score against the antimicrobial ATP synthase, followed by **11g** and **11h**. Notably, the docking scores were lower for the TB target than for the HIV target, consistent with the obtained biological data. The two promising compounds in the anti-TB and anti-HIV biological screenings, and their interaction with the active sites of the proteins were observed, as depicted in **Figure 4**.

 doi:10.20944/preprints202504.0967.v1

The 4V1F enzyme is known to be the target for compounds containing the quinoline moiety, such as mefloquine and bedaquiline, and has been used extensively in molecular docking of quinoline-based compounds [22,43]. Compound **11h** (MIC_{90} = 88.72 μM) displayed a docking score of -2.606 compared to **11a** (MIC_{90} = 186.52 μM), which had a docking score of -2.540. In **Figure 4**, compound **11a** demonstrated hydrogen bond interactions with Glu65, Tyr68, and Phe69 and additional interactions with Ala66, Gly62, Val61, and Phe58 amino acid residues. On the other hand, **11h** exhibited similar interactions with amino acid residues but without any visible hydrogen interaction. Other biological properties of **11h** may contribute further to its biological activity.

Table 3. Docking scores for all synthesised quinoline-1,2,3-triazole-anilines against TB and HIV targets.

Compound	Docking Scores 4V1F	Docking Scores 4MBS
11a	-2.540	-6.990
11b	-2.291	-6.729
11c	-2.339	-6.899
11d	-2.528	-7.561
11e	-2.879	-7.371
11f	-2.035	-4.815
11g	-2.714	-6.427
11h	-2.606	-7.362
11i	-2.479	-5.825
11j	-2.570	-5.301

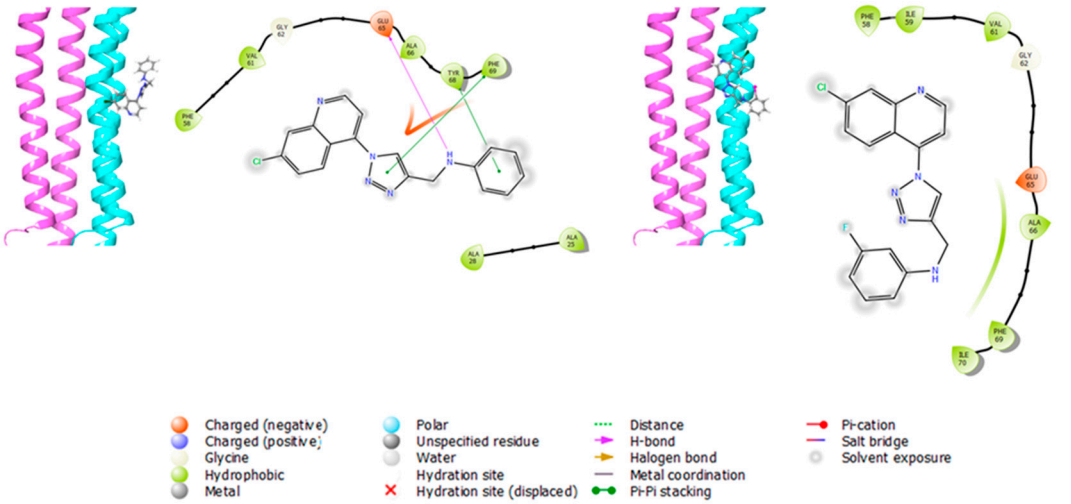

11a **11h**

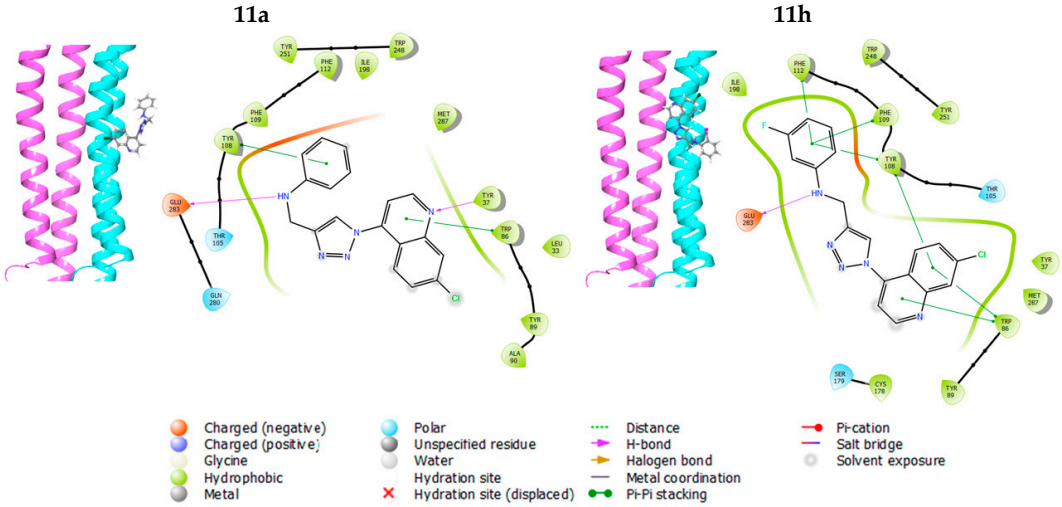

 doi:10.20944/preprints202504.0967.v1

Figure 4. Docking interaction for the most promising compounds **11a** and **11h** (Top - Mtb docking interactions; bottom – antiviral docking interactions).

The selected CCR5 chemokine receptor acts as a co-receptor for HIV-1 viral entry and its associated enzyme (4MBS) is a known target for maraviroc, a triazole-containing antiretroviral [36]. Furthermore, Singh *et al.* [46] and Ibrahim *et al.* [47] reported quinoline-based compounds as chemokine receptor CCR5 inhibitors. Compound **11h** (IC_{50} = 0.01032 μM) demonstrated a significantly higher docking score of -7.362 than **11a** (IC_{50} = 3.013 μM). Hydrogen bonding interactions were observed with various amino acid residues in the active sites; the quinoline and aniline moieties interacted with Phe112, Tyr108, Glu283, and Trp86 for **11h** and **11a**. Further interactions with Tyr89 and Trp248 amino acid residues are observed for both compounds.

2.3.2. Density Functional Theory Studies

The stability of a compound is a consequence of its orbital energies [48]. **Table 4** shows the stability and/or reactivity indices of **11h** at DFT/B3LYP/6-311++G(d,p) level of theory. These reactivity indices are vital for molecular reactivity. The ionisation potential (I) and the electron affinity (A) of **11h** were 5.89 eV and 2.64 eV, respectively. A low I value suggests that a molecule can give up electrons readily [49]. A high value of A implies a good electron-accepting potential for the molecules [49]. The energy gap (Eg) is derived as a difference between the frontier orbital energies. The Eg of 11h was 3.25 eV, while its chemical hardness was 1.63 eV. The global softness was 0.615 eV-1. The ability of a molecule to attract an electron is related to the electronegativity, χ. The χ of 11h was 4.27 eV, while its electrophilicity was 5.59 eV. The values of the reactivity descriptors in 11h here are close to reported bioactive compounds at the same level of theory [50]. Compound 11h can give up electrons easily and also accept electrons from the values of its ionisation potential and electron affinity.

Table 4. The electronic properties and global reactivity descriptors of 11h at the DFT/B3LYP/6-311++G(d,p) level of theory.

Compound	EHOMO (eV)	ELUMO (eV)	I (eV)	A (eV)	Eg (eV)	η (eV)	S (eV-1)	χ (eV)	ω (eV)
11h	-5.89	-2.64	5.89	2.64	3.25	1.63	0.615	4.27	5.59

HOMO, LUMO and ESP surface maps of 11h

The optimised structure, HOMO, LUMO and electrostatic potential maps of **11h** are shown in **Figure 5**. The HOMO map of the compound was spread across the entire fluoroaniline moiety, while the LUMO was delocalised over the other side of the compound (quinoline and triazole rings). This indicates that the compound has the ability to act as an electron donor as well as an acceptor of electrons.

The electrostatic potential (ESP) map (**Figure 6**) accounts for the regions in a molecule prone to nucleophilic and electrophilic attacks. While the red- and yellow-mapped regions show negative electrostatic potential and are prone to attack by an electrophile, the blue- and/or green-mapped regions indicate positive electrostatic potential and are prone to nucleophilic attack.

 doi:10.20944/preprints202504.0967.v1

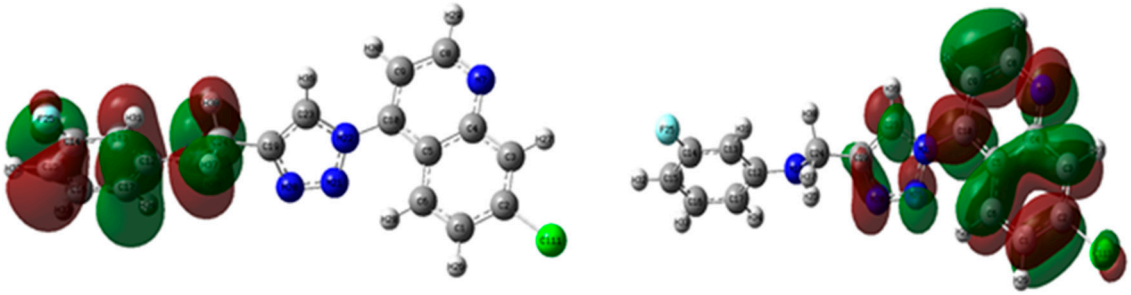

a b

Figure 5. (a) HOMO and (b) LUMO maps of **11h**.

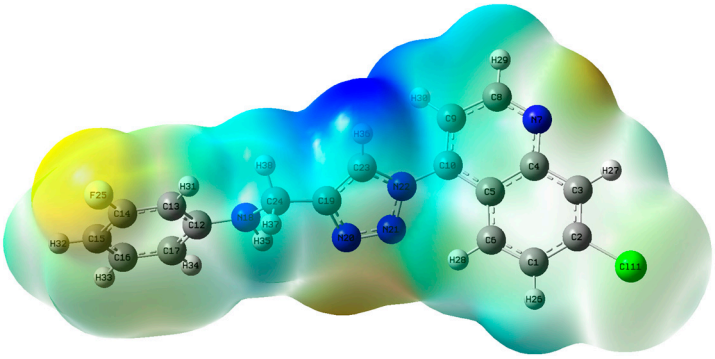

Figure 6. Electrostatic potential map of **11h**.

The sites prone to electrophilic attack in **11h** are the fluorine and chlorine atoms, as well as the quinoline nitrogen. The sites prone to nucleophilic attack are the triazole's C19, C23, N21, N22 and H30 atoms, extending to N18 through C24 and their hydrogen atoms; some faint blue/green maps were seen on other parts of the quinoline rings. The charge separation between these two opposite electrostatic potential sites could facilitate intramolecular charge transfer [51].

2.3.3. ADMET Predictions

Adsorption, distribution, metabolism, excretion and toxicity (ADMET) properties describe a drug's absorption, distribution, metabolism, excretion and toxicity within living organisms [52]. ADMET predictions of the synthesised 1,2,3-triazole-quinoline-aniline compounds were calculated using the QikProp utility in the Schrödinger Suite [45]. The human serum binding ability coefficient (QPlogKhsa) ranged from 0.500 to 0.779, suggesting likely favourable bioavailability and less likely to be protein-bound. The predicted aqueous solubility (QPlogS) values for all but one compound, **11g** (-6.979), were within the acceptable range, suggesting good intestinal absorption.

The predicted percentage of human oral absorption for most compounds was 100%, except for **11i**, which has ~88%, indicating potential excellent oral bioavailability, with >80% being categorised as high. Furthermore, the predicted brain/blood coefficient (QPlogBB) values were also in the accepted range (-0.023 to -1.346), while these compounds were predicted to be likely inactive in the central nervous system (CNS) (< +2). The likely number of metabolic reactions from the cytochrome P450 enzyme was predicted to be less than 7, indicating a favourable outcome. Lastly, most of these compounds adhered to Lipinski's criteria for molecular weight, octanol-water coefficient, and the number of hydrogen bond donors and acceptors, except **11c** and **11g**, which violated this guideline due to their high lipophilicity (clogP) of greater than 5.

 doi:10.20944/preprints202504.0967.v1

Table 5. *In silico* ADMET property predictions of 11a-j.

Compound	QPlogKhsa	QPlogS	% Human oral absorption	QPlogBB	CNS	#metab	Ro5
11a	0.555	-5.804	100.000	-0.293	0	5	0
11b	0.697	-6.667	100.000	-0.127	0	4	0
11c	0.723	-6.793	100.000	-0.116	0	4	1
11d	0.597	-6.169	100.000	-0.186	0	4	0
11e	0.673	-6.548	100.000	-0.137	0	5	0
11f	0.549	-5.946	100.000	-0.329	0	6	0
11g	0.779	-6.922	100.000	-0.022	0	6	1
11h	0.598	-6.169	100.000	-0.187	0	6	0
11i	0.500	-5.932	88.989	-1.381	-2	6	0
11j	0.545	-5.938	100.000	-0.369	0	5	0

QPlogKhsa: prediction of binding to human serum albumin (-1.5 to 1.5); QplogS: Predicted aqueous solubility (-6.5 to 0.5); %Human oral absorption: Predicted human oral absorption on 0 to 100 % (>80% is high and <25% is poor); QplogBB: Predicted brain/blood partition coefficient (-3 to 12.0); CNS: Predicted central nervous system activity on a -2 (inactive) to +2 (active scale); #metab: Number of likely metabolic reactions (1 to 8); Ro5: Number of violation of Lipinski's rule of five (Maximum is 4).

3. Materials and Methods

3.1. Chemistry

All the Chemical reagents used in the synthesis were purchased from Merck South Africa/Sigma Aldrich and I&A Chemicals, with purity ranging from 97-100%. HPLC grade and crude solvents were used. The reaction progress was monitored using a thin layer chromatography (TLC) analysis on aluminium-backed TLC plates (Kiese gel 60 F254 plates, Merck South Africa) and visualised under ultraviolet light (254 nm wavelength) All the synthesised final compounds and some intermediates were purified using the flash-column chromatography on silica gel (0.063-0.200mm) and various solvent systems. Melting point analysis was conducted using an electrothermal IA9100 melting point apparatus on the solid compounds using glass capillary tubes; melting points are recorded in ℃ and are uncorrected. Final compounds and intermediates' functional groups were analysed and confirmed by Fourier Transform Infrared (FTIR) spectroscopy on the Perkin Elmer 100 spectrophotometer with Universal ATR sampling accessory; wavenumbers (υ) on the spectra expressed in cm-1.

Nuclear magnetic resonance (NMR) analysis was conducted on the Bruker Avance III 600 Hz spectrometer using deuterated chloroform ($CDCl_3$) and dimethylsulfoxide (DMSO-d6) and solvents. Topspin was used for spectra analysis; coupling constants (J) were reported in Hertz (Hz) and the chemical shifts in parts per million (ppm) using tetramethyl silane (TMS) peak as reference. The splitting patterns are reported as singlet (s), doublet (d), multiplet (m), triplet (t), quartet (q), doublet of doublets (dd), doublet of triplets (dt), or triplet of doublets (td). The solvent peaks were referenced at 2.50 (^{1}H) and δ 39.5 (^{13}C) for DMSO-d6, and 7.26 (^{1}H) and 77.0 (^{13}C) for $CDCl_3$, while residual water was observed at 3.35 and 1.56 ppm, respectively.

Preparation of N-[1-(7-chloroquinolin-4-yl)-1H-1,2,3-triazol-4-yl]anilines (11a-j)

100 mg (0,77 mmol) of the respective *N*-(prop-2-ny-l-yl)anilines (**10a-j**) and 189 mg (0.92mmol) 7-chloroquinoline-4-azide (**7**) were dissolved in 10mL DCM in a 100 mL round bottom flask. Thereafter, 22% sodium ascorbate, 10% copper sulphate and 10mL of water were added, and the reaction mixture was vigorously stirred at room temperature until completion (24 hrs). On completion, based on TLC, 100mL of water was added, followed by 5 x 40mL DCM extraction, and the combined extracts evaporated *in vacuo* to afford crude compounds, which were purified by column chromatography (DCM: MeOH; 95:5%):

 doi:10.20944/preprints202504.0967.v1

1-(7-Chloro-4-quinolinyl)-1*H*-1,2,3,-triazole-4-methanamine (11a): As a cream white solid, yield 88%, mp 15-152°C, IR (cm^{-1}) C-H 2900-3000, ^{1}H-NMR (DMSO-d6, 600 MHz, ppm) δ_H 4.47 (2H, d, J = 5.7 Hz, H-1), 6.21 (1H, t, J = 5.7 Hz, H-2), 6.58 (1H, t, J = 7.5 Hz, H-5), 6.72 (2H, d, J = 7.9 Hz, H-3 and H-3′), 7.11 (2H, dd, J_1 = 8.3 Hz, J_2 = 7,4 Hz, H-4 and H-4′), 7.78 (1H, dd, J_1=7.0 Hz, J_2= 2 Hz, H-10), 7.8 (1H, d, J = 4.5 Hz, H-7), 8.02 (1H, d, J = 9.1 Hz, H-11), 8.28 (1H, d, J = 2.0 Hz, H-9), 8.74 (1H, s, H-6), 9.14 (1H, d, J = 4.5 Hz, H-8). ^{13}C-NMR (DMSO-d6, 150 MHz, ppm) δ_C 39.9 (C-1), 112.9 (C-3), 116.7 (C-5), 117.3 (C-7), 120.7 (C-15a), 125.7 (C-11), 125.9 (C-6), 128.6 (C-9), 129.4 (C-4,10), 135.8 (C-16), 140.9 (C-14), 147.1 (C-13), 148.7 (C-12), 149.9 (C-15b), 152.8 (C-8). TOFF MS ES-: (*m*/*z*) 306.0968 (100%) [(M-H) - N_2]$^-$ (Calculated for $C_{18}H_{13}ClN_3^-$(306.0803)].

[1-(7-Chloro-4-quinolinyl)-1*H*-1,2,3-triazole-4-methyl]-4-bromoaniline (11b): As a light brown solid, yield 87%, mp 187-190°C, IR (cm^{-1}) C-H 2900-3000; ^{1}H-NMR (DMSO-d6, 600 MHz, ppm) δ_H 4.48 (2H, d, J = 5.2 Hz, H-1), 6.4 (1H, s, H-2), 6.71 (2H, d, J = 8.7 Hz, H-4), 7.25 (2H, d, J =8.7 Hz, H-3), 7.76 (1H, dd, J_1 = 9.0, J_2 = 1.5 Hz, H-10), 7.81 (1H, d, J = 4.6 Hz, H-7), 8.01 (1H, d, J = 9.0 Hz, H-11), 8.26 (1H, d, J = 1.5 Hz, H-9), 8.74 (1H, s, H-6), 9.14 (1H, d, J = 4.5 Hz, H-8). ^{13}C-NMR (DMSO-d6, 150 MHz, ppm) δ_C 38.0 (C-1)114.0 (C-4), 131.0 (C-3), 117.3 (C-7), 120.7 (C-15a), 125.6 (C-6), 125.8 (C-11), 128.6 (C-9), 129.4 (C-10), 135.8 (C-16), 140.9 (C-14), 148.0 (C-12), 147.0 (C-13), 149.8 (C-15b), 152.0 (C-8), 107.0 (C-5). TOF MSMS ES-: (*m*/*z*) 451.4776 [(M^- + HCl]$^-$ [Calculated for $C_{18}H_{19}BrCl_2N_5$ (451.1490)].

[1-(7-Chloro-4-quinolinyl)-1*H*-1,2,3-triazole-4-methyl]-4-iodoaniline (11c): As a brown solid, yield 92%, mp 195-199 °C, IR (cm^{-1}) C-H 2900-; ^{1}H-NMR (DMSO-d6, 600 MHz, ppm) δ_H 4.45 (2H, d, J =5.5 Hz, H-1), 6.47 (1H, t, J = 5.5 Hz, H-2), 6.58 (2H, d, J = 8.7 Hz, H-4), 7.37 (2H, d, J = 8.7 Hz, H-3), 7.78 (1H, dd, J_1 = 9.0, J_2 = 1.9 Hz, H-10), 7.81 (1H, d, J = 4.5 Hz, H-7), 7.99 (1H, d, J = 8.8 Hz, H-11), 8.28 (1H, s, H-9), 8.72 (1H, s, H-6), 9.15 (1H, s, H-8). ^{13}C-NMR (DMSO-d6, 150 MHz, ppm) δ_C 39.0 (C-1), 137.6 (C-3),117.3 (C-7), 77.4 (C-5), 120.7 (C-15a), 125.6 (C-6), 125.9 (C-11), 128.5 (C-9), 129.3 (C-10), 115.8 (C-4), 135.7 (C-16), 140.9 (C-14), 137.9 (C-12), 147.1 (C-13), 149.8 (C-15b), 152.8 (C-8). TOFF MS ES-: (*m*/*z*) [(M + Cl]$^-$ 495.9821 (100%) (Calculated for $C_{18}H_{13}Cl_2N_5^-$(495.9593)].

[1-(7-Chloro-4-quinolinyl)-1*H*-1,2,3-triazole-4-methyl]-4-flouroaniline (11d): As a light grey solid, yield 79%, mp-145-148, IR (cm^{-1}) C-H 2900-3000, ^{1}H-NMR (DMSO-d6, 600 MHz, ppm) δ_H 4.44 (2H, d, J = 5.2 Hz, H-1), 6.15 (1H, t, J = 5.6 Hz, H-2), 6.71 (2H, dd, J1 = 9.1 Hz, J2 = 4.4 Hz, H-4), 6.96 (2H, t, J = 9.1 Hz, H-3), 7.79 (1H, dd, J_1 = 9.0 Hz, J_2 = 1.5 Hz, H-10), 7.82 (1H, d, J = 4.5 Hz, H-7), 8.01 (1H, d, J = 9.0, H-11), 8.29 (1H, d, J = 1.5 Hz, H-9), 8.73 (1H, s, H-6), 9.15 (1H, d, J = 4.5 Hz, H-8). ^{13}C-NMR (DMSO-d6, 150 MHz, ppm) δ_C 39.0 (C-1), 113.7 (C-4), 115,8 (C-3), 117.3 (C-7), 120.7 (C-15a), 125.6 (C-6), 125.8 (C-11), 128.6 (C-9), 129.4 (C-10), 135.8 (C-16), 140.9 (C-14), 145.4 (C-12), 147.0 (C-13), 149.8 (C-15b), 152 (C-8), 154.3/155.8 (C-5). TOFF MS ES-: (*m*/*z*) [(M-H) - N_2]- 324.0866 (100%) (Calculated for $C_{18}H_{12}ClFN_3^-$(324.0709)].

[1-(7-Chloro-4-quinolinyl)-1*H*-1,2,3-triazole-4-methyl]-3-chloroaniline (11e): As a yellow solid, yield 69%, mp 169-172 °C, IR (cm^{-1}) C-H 2900-3000, ^{1}H-NMR (DMSO-d6, 600 MHz, ppm) δ_H 4.48 (2H, d, J = 5.6 Hz, H-1), 6.53 (1H, t, J=Hz, H-2), 6.66 (H, t, J = 8.0 Hz, H-5), 6.74 (1H, s, H-3′), 6.74 (1H, dd, J_1 = 3 Hz, J_2 = 2.4 Hz H-4′), 7.10 (1H, dd, J_1 = 9.2 Hz, J_2 =1.9 Hz, H-3), 7.12 (1H, s, H-3), 7.80-7.79 (2H, m, H-7 and H-10), 8.01 (1H, d, J = 9.0 Hz, H-11), 8.27 (1H, d, J = 1.6 Hz, H-9), 8.72 (1H, s, H-6), 9.13 (1H, d, J = 4.5 Hz, H-8). ^{13}C-NMR (DMSO-d6, 150 MHz, ppm) δ_C 38.6 (C-1), 112.1 (C-3), 111.5(C-3′), 117,3 (C-7), 130.8 (C-5), 120.7 (C-15a), 125.7 (C-6), 125.8 (C-11), 128.6 (C-9), 129.3 (C-10), 124.7 (C-4′), 135.8 (C-16), 134.1 (C-4), 140.9 (C-14), 150.2 (C-12), 147.0 (C-13), 149.8 (C-15b), 152.8 (C-8). TOFF MS ES-: (*m*/*z*) [(M-H) - N_2]$^-$ 340.0580 (100%) (Calculated for $C_{18}H_{12}Cl_2N_3^-$(340.0414)].

[1-(7-Chloro-4-quinolinyl)-1*H*-1,2,3-triazole-4-methyl]-2-methoxyaniline (11f): As a brown liquid, yield 43%, IR (cm^{-1}) C-H 2900-3000 ^{1}H-NMR (DMSO-d6, 600 MHz, ppm) δ_H 3.79 (3H, s, H-3′′), 4.52 (2H, d, J = 6 Hz, H-1), 5.46 (1H, t, J = 6 Hz, H-2), 6.59 (1H, td, J_1 = 7.7 Hz, J_2 = 1.4 Hz, H-5), 6.72 (1H, dd, J_1 = 7.7 Hz, J_2 = 1.4, H-3′), 6.78 (1H, d, J = 8.0 Hz, H-4), 6.83 (1H, td, J_1 = 7.7 Hz, J_2 = 0.6 Hz, H-4′), 7.76 (1H, dd, J_1 = 9.1 Hz, J_2 = 2.1 Hz, H-10), 7.81 (1H, d, J = 4.6 Hz, H-7), 8.01 (1H, d, J = 9.1 Hz, H-11), 8.26 (1H, d, J = 2.0 Hz, H-9), 8.69 (1H, s, H-6), 9.12 (1H, d, J = 4.6 Hz, H-8). ^{13}C-NMR (DMSO-d6, 150 MHz, ppm) δ_C 39.0 (C-1), 110.2 (C-3′), 138.0 (C-3), 117,3 (C-7), 116.7 (C-5), 120.7 (C-15a), 125.6 (C-6), 125.9 (C-11), 128.5 (C-9), 129.3 (C-10), 110.3 (C-4), 135.7 (C-16), 121.4 (C-4′), 140.9 (C-14), 137.9 (C-

 doi:10.20944/preprints202504.0967.v1

12), 147.1 (C-13), 149.8 (C-15b), 152.8 (C-8), 55.7 (C-3''). TOF MSMS ES$^+$: (*m*/*z*) 388.1096 (M+Na)$^+$ [Calculated for C19H16ClN5NaO (388.0941)].

[1-(7-Chloro-4-quinolinyl)-1*H*-1,2,3-triazole-4-methyl]-2-triflouromethylaniline (11g): As a yellow liquid, yield 48%, IR (cm^{-1}) C-H 2900-3000 ^{1}H-NMR(DMSO-d6, 600 MHz, ppm) δ_H 4.65 (2H, d, J = 5.7 Hz, H-1), 6.11 (1H, s, H-2), 6.73 (1H, t, J = 7.5 Hz, H-5), 7.01 (1H, d, J = 8.4 Hz, H-3'), 7.43 (1H, m, H-4,4'), 7.76 (1H, dd, J_1 = 9.0 Hz, J_2 = 2.0 Hz, H-10), 7.80 (1H, d, J = 4.6 Hz, H-7), 7.96 (1H, d, J = 9.0 Hz, H-11), 8.25 (1H, d, J = 2.0, H-9), 8.65 (1H, s, H-6), 9.11 (1H, d, J = 4.6 Hz, H-8). ^{13}C-NMR (DMSO-d6, 150 MHz, ppm) δ_C 39.0 (C-1), 145.4 (C-3), 112.9 (C-3'), 117.4 (C-7), 116.2 (C-5), 120.7 (C-15a), 126.1 (C-6), 125.8 (C-11), 128.5 (C-9), 129.3 (C-10), 126.7 (C-4'), 135.8 (C-16), 134.0 (C-4), 140.9 (C-14), 146.5 (C-12), 146.5 (C-13), 149.8 (C-15b), 152.8 (C-8),126 (C-3'').

[1-(7-Chloro-4-quinolinyl)-1*H*-1,2,3-triazole-4-methyl]-3-flouroaniline (11h): As a crem white solid, yield 85%, mp 145-148 ℃, IR (cm^{-1}) C-H 2900 ^{1}H-NMR (DMSO-d6, 600 MHz, ppm) δH 4.47 (2H, d, J = 5.7 Hz, H-1), 5.40 (1H, s, H-2), 6.35 (1H, td, J_1 = 8.6, J_2= 2 Hz, H-4), 6.49 – 6.55 (3H, m, H-3, H-3' and H5), 7.76 (1H, dd, J1 = 9.0 Hz, J2 = 1.9 Hz, H-10), 7.80 (1H, d, J = 4.7 Hz, H-7), 8.00 (1H, d, J = 9.2 Hz, H-11), 8.28 (1H, s, Hz, H-9), 8.72 1(H, s, H-6), 9.13 (1H, d, J = 4.6 Hz, H-8). ^{13}C-NMR (DMSO-d6, 150 MHz, ppm) δ_C 38.7 (C-1), 99.2 (C-3), 109.2 (C-3'), 117.3 (C-7), 130.7 (C-5), 143.5 (C-4') 120.7 (C-15a), 125.6 (C-6), 125.9 (C-11), 128.5 (C-9), 129.4 (C-10), 135.8 (C-16), 165.1(C-4), 140.9 (C-14), 153.5 (C-12), 146.6 (C-13), 149.8 (C-15b), 152.8 (C-8). TOFF MS ES$^-$: (*m*/*z*) [(M-H) - N_2]- 324.0868 (100%) (Calculated for $C_{18}H_{12}ClFN_3^-$(324.0709)].

[1-(7-Chloro-4-quinolinyl)-1H-1,2,3-triazole-4-methyl]-3-nitroaniline (11i): As a orange solid, yield 79%, mp 192-197 ℃, IR (cm^{-1}) C-H 2900-3000. ^{1}H-NMR(DMSO-d6, 600 MHz, ppm) δ_H 4.58 (2H, d, J = 5.7 Hz, H-1), 7.00 (H, s, H-2), 7.15 (1H, d, J = 7.74 Hz, H-3'), 7.37 (2H, m, H-4' and H-5), 7.52 (1H, d, J = 7.7 Hz, H-3), 7.77 (1H, t, J = 2.0 Hz, H-10), 7.78 (1H, dd, J_1 = 8.7 Hz, J_2 = 2, H-7), 7.81 (H, dd, J_1 = 9.0 Hz, J_2 = 1.5 Hz, H-11), 8.29 (1H, d, J = 2 Hz, H-9), 8.77 (1H, s, H-6), 9.14 (1H, d, J = 4.5 Hz, H-8). ^{13}C-NMR (DMSO-d6, 150 MHz, ppm) δ_C 39.1 (C-1), 130 (C-4'), 106 (C-3'), 117.4 (C-7), 119.1 (C-3) 120.8 (C-15a), 125.8 (C-6), 125.8 (C-11), 128.6 (C-9), 129.4 (C-10), 135.8 (C-16), 140.9 (C-14), 145.4 (C-12), 146.2 (C-13), 149.81 (C-4), 149.8 (C-15b), 152 (C-8), 111.0 (C-5). TOF MSMS ES$^+$: (*m*/*z*) 381.2533 (M+1)$^-$ [Calculated for $C_{18}H_{14}ClN_6O_2$ (381.7920)].

[1-(7-Chloro-4-quinolinyl)-1*H*-1,2,3-triazole-4-methyl]-4-methoxyaniline (11j): As a brown solid, yield 86%, mp-xx, IR (cm^{-1}) C-H 2900-3000. ^{1}H-NMR(DMSO-d6, 600 MHz, ppm) δ_H 3.64 (3H, s, H-5'), 4.42 (2H, d, J = 5.8 Hz, H-1), 5.76 (1H, t, J = 5.8 Hz, H-2), 6.68 (2H, d, J = 8.8 Hz, H-4), 6.74 (2H, d, J = 8.8 Hz, H-3), 7.75 (1H, dd, J_1 = 9.0 Hz, J_2 = 1.8 Hz, H-10), 7.79 (1H, d, J = 4.6 Hz, H-7), 8.01 (1H, d, J = 9.0 Hz, H-11), 8.25 (1H, d, J = 1.7 Hz, H-9), 8.68 (1H, s, H-6), 9.11 (1H, d, J = 4.6 Hz, H-8). ^{13}C-NMR (DMSO-d6, 150 MHz, ppm) δ_C 40.4 (C-1), 115.07 (C-3), 117.2 (C-7), 151.6 (C-5), 55.7 (C-5'), 120.7 (C-15a), 125.6 (C-6), 125.9 (C-11), 128.5 (C-9), 129.3 (C-10), 135.7 (C-16), 114.1 (C-4), 140.9 (C-14), 142.9 (C-12), 147.1 (C-13), 149.8 (C-15b), 152.8 (C-8). TOFF MS ES$^-$: (*m*/*z*) [(M-H) - N_2]- 336.1097 (100%) [Calculated for $C_{19}H_{15}ClN_3O^-$ (336.0909)].

3.2. Biology

3.2.1. Antimycobacterial Evaluation

In vitro antimycobacterial evaluation assay was performed against the H37Rv strain using the previously reported procedure [22]. Cultured H37Rv (ATCC 27294) in Middlebrook 7H9 (Difco) broth supplemented with 0.1 % glycerol (Merck) and 10 % oleic acid-albumin-dextrose-catalase (OADC) (Becton-Dickenson) were aerobically grown at 37 °C until an optical density (OD)600nm of 1 was attained. This was equivalent to approximately 3 x 108 bacilli/mL.

The antimicrobial activity of the various compounds was tested in triplicates using micro broth dilution assays in 96 well plates. These plates were sealed and incubated at 37 °C for 7 days and microbial growth was measured by observing the resazurin colour change from blue to pink. The minimum inhibitory concentration (MIC) was interpreted as the lowest concentration inhibiting a colour change from blue to pink.

 doi:10.20944/preprints202504.0967.v1

3.2.2. MTT Cytotoxicity Evaluation

In vitro cytotoxicity evaluation assay was performed on the TZM-bl cell line, a HeLa cell line clone, as previously reported [22]. The cell were seeded at a density of 25000 (DEAE dextran 44 µl/10ml) cells + 150µl DMEM/well in a 96-well microtiter plate, in duplicates and incubated overnight for attachment (37°C, 5% CO_2). Treatments (2.5mg/ml) were prepared and following incubation, the supernatant (treatment medium) was removed, and 120 µl of MTT solution comprising 100µl fresh CCM and 20µl of MTT (5mg/ml MTT salt in 0.1M PBS) was added to each well. The plate was then incubated for 4 hours (37°C, 5% CO_2). The optical density of each sample was measured at 450 using a microplate reader (Perkin Elmer). The maximum inhibitory concentration resulting in 50% cytotoxicity concentration (CC_{50}) was obtained using GraphPad Prism version 5.01 by plotting a dose-response curve (concentration versus the percentage cell viability of the samples). (*see cytotoxicity dose-response curved in the supplementary information*).

3.2.3. Luciferase-Based Antiviral Assay Evaluating Human Immunodeficiency Virus

Maintenance of Cell Lines

In sterile 75 cm2 culture flasks, the TZM-bl cell lines (NIH AIDS Research and Reference Reagents Programme) were cultured as a monolayer using Dulbecco's Modified Eagle Medium (DMEM) (Thermo Fisher Scientific, Waltham, MA, USA) supplemented with 10% fetal bovine serum (FBS; heat-inactivated and gamma irradiated) (LTC Biosciences, Gainesville, FL, USA), 25 mM of HEPES (Thermo Fisher Scientific, Waltham, MA, USA), and 50 µL/mL of gentamicin (Thermo Fisher Scientific, Waltham, MA, USA). A HeLa cell line clone, the TZM-bl cell line is altered to produce CD4 and CCR5, enabling HIV-1 infection and firefly luciferase regulated by the HIV-1 long-terminal repeat (LTR) [53].

Antiviral Assay

The HIV-1 inhibition of synthesised drugs was evaluated using a Luciferace-based antiviral assay [54]. Initially, 96-well cell culture plates were filled with 150 uL, 100 uL, and 140 uL of DMEM; test compound, viral control, and cell control were added, respectively. Briefly, 96-cell culture well plates (Corning Costar, New York, NY, USA) were filled with 11 uL of AZT drug (positive control) and test compounds. The plates were then diluted three times in 140 uL of DMEM supplemented with 10% FBS, 25% HEPES buffer, and 1% penicillin-streptomycin. 10,000 TZM-bl cell lines were infected with 50 uL NL4.3 virus (subtype B) in 96 well culture plates. Experimental controls included infected (virus control) and uninfected (cell control) TZM-bl cell line, which was incubated for an hour. After adding 10,000 cells to each 96-well plate, the cells were grown for 48 hours at 37 °C, 5% CO_2, 95% humidity, and 37.5 ug/mL of DEAE-dextran. 150 ul of medium was taken out and replaced with 100 uL of the Bright-Glo TM luciferase reagent without light exposure following a 48-hour incubation period. After aspirating the supernatant, 150 uL of the mixture containing the Bright-Glo TM luciferase reagent was put into a Corning Costar 96-well black plate. It was measured right away at 540 nm in the Victor Nivo microplate reader (PerkinElmer, Waltham, USA). Then, the percentage of viral inhibition was calculated as follows:

$$\% \text{ HIV inhibition} = (\text{average sample} - \text{average control})/(1 - (\text{average viral control} - \text{average control}) \times 100 \quad (1)$$

The results of the absorbance-based quantification of the viral cell were through the inhibitory concentration at 50% was obtained by plotting the dose-response curve (log concentration versus % HIV inhibition) (*see HIV assay dose-response curved in the supplementary information*).

3.3. In Silico Studies

3.3.1. Molecular Docking

 doi:10.20944/preprints202504.0967.v1

The compounds and proteins were prepared using the ligand preparation (LigPrep) and protein preparation wizard modules [55] (on Maestro software in Schrödinger Suite [45]). The compounds were docked at the active sites of the proteins.

3.3.2. DFT Studies

The structure of 11h was optimised at the DFT/B3LYP/6-311++G(d,p) level of theory in the gas phase. Frequency calculations of the optimised structure were performed to ensure that the geometry conforms to minima. The ionisation potential and electron affinity were calculated from the frontier molecular orbital energies (EHOMO) and (ELUMO), respectively [56]. Other reactivity indices such as the energy gap (Eg), chemical hardness and softness (η and S, respectively), electronegativity (χ) and electrophilicity (ω) were all calculated [57]; see equations 1-8. The distribution of the molecular orbitals over the molecular surface was visualised via the HOMO and LUMO maps [51]. An electrostatic potential (ESP) map was used to visualise the selective reactive sites of interaction of 11h with an electron donating or withdrawing neighbour [58].

$$I = -E_{HOMO} \quad (2)$$

$$A = -E_{LUMO} \quad (3)$$

$$E_g = E_{LUMO} - E_{HOMO} \quad (4)$$

$$\eta = \frac{I - A}{2} \quad (5)$$

$$S = \frac{1}{\eta} \quad (6)$$

$$\chi = \frac{I + A}{2} \quad (7)$$

$$\omega = \frac{(I+A)^2}{8\eta} = \frac{\chi^2}{2\eta} \quad (8)$$

4. Conclusions

Applying molecular hybridisation, new quinoline-1,2,3-triazole-anilines were successfully synthesised in moderate to excellent yields. Their structures were confirmed using spectroscopic and spectrometric techniques. The synthesised compounds demonstrated moderate to negligible activity against *Mtb in vitro*. However, notable anti-HIV activity was observed in compounds **11g**, **11h** and **11i**, with their IC_{50} being 0.3883 μM, 0.0103 μM and 0.167 μM, respectively, with **11h** exhibiting the best activity against both *Mtb* and HIV. Furthermore, **11h** showed 9-fold superior activity than the reference drug, AZT (0.0909 μM).

Additionally, the presence of fluoride in certain compounds appears to have improved antiviral activity. Cytotoxicity assessments generally revealed low toxicity except for a few compounds. Selective indices (SI) of **11g** and **11h** are 11367 and 2472.87, respectively, suggesting that these compounds would pose less cytotoxic effects in vivo. Molecular docking studies revealed that **11h** interacted with some of the essential amino acid residues in the active site of the HIV-1 co-receptor entry enzyme. The DFT studies on **11h** revealed reactivity and reactive sites in the compound, while the predicted ADMET parameters for most compounds indicated drug-like molecules. Thus, 11h is a potential hit for further optimisation studies against HIV-1.

 doi:10.20944/preprints202504.0967.v1

Supplementary Materials: The following are available online [Cell viability plot, ^{1}H and ^{13}C NMR and 2D-NMR spectra of the synthesised target compounds, IR spectra, MS data, cytotoxicity assay dose-response curves and HIV assay dose-response curves).

Author Contributions: Methodology, formal analysis, writing-original draft, S.S.M.; Methodology, formal analysis, writing-reviewing & editing, D.N.; Methodology, formal analysis, validation, writing-reviewing & editing, O.E.O.; Methodology, formal analysis, writing-reviewing & editing, S.S.; Conceptualization, supervision, formal analysis, funding acquisition, writing-reviewing & editing, N.P.M.; Conceptualization, supervision, project administration, funding acquisition, formal analysis, writing-reviewing & editing, M.T. All authors have read and agreed to the published version of the manuscript.

Funding: The South African National Research Foundation (NRF)'s Competitive Support for unrated research grants [CSUR: 116285(M.T.)], South African Medical Research Council Self-Initiated Research (N.P.M.), and UKZN are gratefully acknowledged for financial and other valuable support. Tertiary Education Trust Fund (TETFUND), from the Government of the Republic of Nigeria, for the Postdoctoral Fellowship Award (TETF/ES/UNIV/ONDO STATE/TSAS/2021) (O.E.O.). The content of this publication is solely the responsibility of the authors and does not necessarily represent the official views of the funders.

Acknowledgments: All computational calculations were carried out using resources at the Centre for High-Performance Computing (CHPC), Cape Town, South Africa.

Institutional Review Board Statement: Not applicable

Informed Consent Statement: Not applicable

Data availability: Original experimental data not provided in the supplementary information are available from the authors on request.

Conflicts of Interest: The authors declare no conflict of interest.

References

1. Global Tuberculosis Report 2024. *World Health Organisation*: Geneva, **2024**. https://iris.who.int/bitstream/handle/10665/379339/9789240101531-eng.pdf?sequence=1 (Accessed on 17 January 2025).
2. Quimque, M.T.G.; Go, A.D.; Lim, J.A.K.; Vidar, W.S.; Macabeo, A.P.G. Mycobacterium tuberculosis Inhibitors Based on arylated quinoline carboxylic acid backbones with anti-Mtb gyrase activity. *Int. J. Mol. Sci*. 2023, 24 (14), 11632. https://doi.org/10.3390/ijms241411632
3. Martinez, R.M. Bacillus subtilis, in Brenner's Encyclopedia of Genetics (2nd Ed), S. Maloy and K. Hughes, Editors. **2013**, *Academic Press*: San Diego, 246-248.
4. Smith, T., Wolff, K.A.; Nguyen, L. Molecular biology of drug resistance in Mycobacterium tuberculosis. *Curr. Top. Microbiol. Immunol*. **2013**. 374: p. 53-80. https://doi.org/10.1007/82_2012_279
5. Sawyer, E.B.; Grabowska, A.D.; Cortes, T. Translational regulation in mycobacteria and its implications for pathogenicity. *Nucleic Acids Res*. **2018**, 46(14): 6950-6961. https://doi.org/10.1093/nar/gky574
6. Bhat, Z.S.; Rather, M.A.; Maqbool, M.; Ahmad, Z. Drug targets exploited in Mycobacterium tuberculosis: Pitfalls and promises on the horizon. *Biomed. Pharmacother*. **2018**, 103, 1733-1747. https://doi.org/10.1016/j.biopha.2018.04.176
7. Amusengeri, A.; Khan, A.; Tastan Bishop, O. The structural basis of Mycobacterium tuberculosis RpoB drug-Resistant clinical mutations on rifampicin drug binding. *Molecules*, **2022**, 27(3), 885. https://doi.org/10.3390/molecules27030885
8. Goldberg, D.E.; Siliciano, R.F.; Jacobs, W.R. Outwitting evolution: Fighting drug-resistant TB, malaria, and HIV. *Cell*, **2012**, 148(6), 1271-1283. https://doi.org/10.1016/j.cell.2012.02.021
9. Aguilar Diaz, J.M.; Abulfathu, A.A.; te Brake, L.H.M.; van Ingen, J.; Kuipers, S.; Magis-Escurra, C.; Raiijmaker, J.; Svensson, E.M., Boeree, M.J. New and repurposed drugs for the treatment of active tuberculosis: An Update for clinicians. *Respiration*, **2023**, 102(2), 83-100. https://doi.org/10.1159/000528274
10. Rendon, A.; Tiberi, S.; Scardigli, A.; D'Ambrosio, L.; Centis, R.; Caminero, J.A.; Migloori, G.B. Classification of drugs to treat multidrug-resistant tuberculosis (MDR-TB): evidence and perspectives. *J. Thorac. Dis*. **2016**, 8(10), 2666-2671. https://doi.org/10.21037/jtd.2016.10.14
11. Karim, Q.A.; Karim, S.S.A. The evolving HIV epidemic in South Africa. *Int. J. Epidemol*. **2002**, 31(1), 37-40. https://doi.org/10.1093/ije/31.1.37

 doi:10.20944/preprints202504.0967.v1

12. The urgency of now: AIDS at a crossroads, *Joint United Nations Programme on HIV/AIDS*: Geneva, **2024**. https://www.unaids.org/sites/default/files/media_asset/2024-unaids-global-aids-update_en.pdf (accessed 17 March 2025).
13. Maeda, K.; Das, D.; Kobayakawa, T.; Tamamura, H.; Takeuchi, H. Discovery and development of anti-HIV therapeutic agents: Progress towards improved HIV medication. *Curr. Top. Med. Chem*. **2019**, 19(18), 1621-1649. https://doi.org/10.2174/1568026619666190712204603
14. Phanuphak, N.; Gulick, R.M. HIV treatment and prevention 2019: Current standards of care. *Curr. Opin. HIV AIDS*, **2020**, 15(1), 4-12. https://doi.org/10.1097/COH.0000000000000588
15. Arts, E.J.; Hazuda, D.J. HIV-1 antiretroviral drug therapy. *Cold Spring Harb. Perspect. Med*. **2012**, 2(4): a007161. https://doi.org/10.1101/cshperpspect.a007161
16. Holec, A.D.; Mandal, S.; Prathipati, P.K.; Destache, C.J. Nucleotide reverse transcriptase inhibitors: A thorough review, present status and future perspective as HIV therapeutics. *Curr. HIV Res*. **2017**, 15(6), 411-421. https://doi.org/10.2174/1570162X15666171120110145
17. Koren, D.E.. 225 Classes of antiretrovirals, in Fundamentals of HIV Medicine. **2020**, *Oxford University Press*, New York. 225-238
18. Di, L. and E.H. Kerns. Drug-like properties: Concepts, structure design and methods from ADME to toxicity optimization. **2012**, *Academic Press,* Califonia.
19. Sluis-Cremer, N.; Tachedjian, G. Mechanisms of inhibition of HIV replication by non-nucleoside reverse transcriptase inhibitors. *Virus Res*. **2008**, 134(1-2), 147-156. https://doi.org/10.1016/j.virusres.2008.01.002
20. Ramprasad, J.; Sthalam, V.K.; Thampunuri, R.L.M.; Bhukya, S.; Ummanni, R.; Balasubramanian, S.; Pabbaraja, S. Synthesis and evaluation of a novel quinoline-triazole analogs for antitubercular properties via molecular hybridization approach. *Bioorg. Med. Chem. Lett.* **2019**, 29(20), 126671. https://doi.org/10.1016/j.bmcl.2019.126671
21. Thomas, K.D.; Adhikari, A.V.; Chowdhury, I.H.; Sumesh, E.; Pal, N.K. New quinolin-4-yl-1,2,3-triazoles carrying amides, sulphonamides and amidopiperazines as potential antitubercular agents. *Eur. J. Med. Chem*. **2011**, 46 (6), 2503-2512. https://doi.org/10.1016/j.ejmech.2011.03.039
22. Nyoni, N.T.P.; Ncube, N.B.; Kubheka, M.X.; Mkhwanazi, N.P.; Senzani, S.; Tukulula, M. Synthesis, characterization, in vitro antimycobacterial and cytotoxicity evaluation, DFT calculations, molecular docking and ADME studies of new isomeric benzimidazole-1,2,3-triazole-quinoline hybrid mixtures. *Bioorg. Chem*. **2023**, 141: 106904. https://doi.org/10.1016/j.bioorg.2023.106904
23. Reddyrajula, R.; Dalimba, U. Quinoline-1,2,3-triazole hybrids: Design and synthesis through Click Reaction, evaluation of antitubercular activity, molecular docking and in silico ADME studies. *ChemistrySelect*, **2019**, 4(9), 2685-2693. https://doi.org/10.1002/slct.201803946
24. Ganesan, M.S.; Raja, K.K.; Murugesan, S.; Karankumar, B.; Faheem, F.; Thirunavukkarasu, S.; Shetye, G.; Ma, R.; Franzablau, S.G.; Wan, B.; Rajagopal, J. Quinoline-proline, triazole hybrids: Design, synthesis, antituberculosis, molecular docking, and ADMET studies. *J. Heterocycl. Chem*. **2021**, 58(4), 952-968. https://doi.org/10.1002/jhet.4229
25. Yadav, J.; Kaushik, C.P. Quinoline-1,2,3-triazole hybrids: Design, synthesis, antimalarial and antimicrobial evaluation. *J. Mol. Struct*. **2024**, 1316: 138882. https://doi.org/10.1016/j.molstruc.2024.1388882
26. Thakare, P.P.; Shinde, A.D.; Chavan, A.P.; Nyayanit, N.V.; Bobade, V.D.; Mhaske, P.C. Synthesis and biological evaluation of new 1,2,3-triazolyl-pyrazolyl-quinoline derivatives as potential antimicrobial agents. *ChemistrySelect*, **2020**, 5(15), 4722-4727. https://doi.org/10.1002/slct.201904455
27. Jamshidi, H.; Naimi-Jamal, M.R.; Safavi, M.; Sanati, K.R.; Azerang, P.; Tahhighi, A. Synthesis and biological activity profile of novel triazole/quinoline hybrids. *Chem. Biol. Drug Des.* **2022**, 100(6), 935-946. https://doi.org/10.1111/cbdd.14031
28. Bhoye, M.R.; Shinde, A.; Shaik, A.L.N.; Shisode, V.; Chavan, A.; Maliwal, D.; Pisssurlenkar, R.R.S. New thiazolyl-isoxazole derivatives as potential anti-infective agents: design, synthesis, in vitro and in silico antimicrobial efficacy. *J. Biomol. Struct. Dynamic*. **2024**, 23, 1-15. https://doi.org/10.1080/07391102.2024.2306497
29. Costa, C.C.P.; Boechat, N.; Bastos, M.M.; da Silva, F-de.C.; Marttorelli, A.; Souza, T.M.L; Baptista, M.S.; Hoelz, L.V.B.; Caffarena, E.R. New efavirenz derivatives and 1,2,3-triazolyl-phosphonates as inhibitors of

 doi:10.20944/preprints202504.0967.v1

reverse transcriptase of HIV-1. *Curr. Top. Med. Chem*. **2018**, 18(17), 1494-1505. https://doi.org/10.2174/1568026618666181029150118

30. Feng, L.S.; Zheng, M-J.; Zhao, F.; Liu, D. 1,2,3-Triazole hybrids with anti-HIV-1 activity. *Arch. Pharm*. **2021**, 354(1), e2000163. https://doi.org/10.1002/ardp.202000163
31. Tian, Y., Liu, Z.; Huang, B.; Kang, D.; Zhang, H.; De Clercq, E.; Daelemans, D.; Pannecouque, C.; Leé, K-H.; Chen, C-H.; Zhan, P.; Liu, Z. Targeting the entrance channel of NNIBP: Discovery of diarylnicotinamide 1,4-disubstituted 1,2,3-triazoles as novel HIV-1 NNRTIs with high potency against wild-type and E138K mutant virus. *Eur. J. Med. Chem*. **2018**, 151, 339-350. https://doi.org/10.1016/j.ejmech.2018.03.059
32. Zhou, Z.; Liu, T.; Wu, G.; Kang, D.; Fu, Z.; Wang, Z.; De Clercq, E.; Pannecouque, C.; Zhan, P. Liu, X. Targeting the hydrophobic channel of NNIBP: discovery of novel 1,2,3-triazole-derived diarylpyrimidines as novel HIV-1 NNRTIs with high potency against wild-type and K103N mutant virus. *Org. Biomol. Chem*. **2019**, 17, 3202-3217. https://doi.org/10.1039/C9OB00032A
33. Ahmad, A.; Akthar, J.; Ahmad, M.; Khan, M.I.; Wasim, R.; Islam, A.; Singh. A. Bedaquiline: An Insight Into its clinical use in multidrug-resistant pulmonary tuberculosis. *Drug. Res.* **2024**, 74(6), 269-279. https://doi.org/10.1055/a-2331-7061
34. Sutherland, H.S.; Tong, A.S.T.; Choi, P.J.; Blaser, A.; Conobe, D.; Franzblau, S.G.; Lotlikar, M.U.; Cooper, C.B.; Upton, A.M.; Denny, W.A.; Palmer, B.D. 3,5-Dialkoxypyridine analogues of bedaquiline are potent antituberculosis agents with minimal inhibition of the hERG channel. *Bioorg. Med. Chem*. **2019**, 27(7), 1292-1307. https://doi.org/10.1016/j.bmc.2019.02.026
35. Emu, B.; Fessel, J.; Schrader, S.; Kumar, P.; Richmond, G.; Win, S.; Weinheimer, S. Marsolais, C.; Lewis, S. Phase 3 study of ibalizumab for multidrug-resistant HIV-1. *N. Engl. J. Med*. **2018**, 379(7), 645-654. https://doi.org/10.1056/NEJMoa1711460
36. Xu, G.G.; Guo, J.; Wu, Y. Chemokine Receptor CCR5 antagonist Maraviroc: Medicinal chemistry and clinical applications. *Curr. Top. Med. Chem*. **2014**, 14(13), 1504-1514. https://doi.org/10.2174/1568026614666140827143745
37. Price, D.A.; Armour, D.; de Groot, M.; Leishman, D.; Napier, C.; Perros, M.; Stammen, B.L.; Wood, A. Overcoming hERG affinity in the discovery of maraviroc; a CCR5 antagonist for the treatment of HIV. *Bioorg. Med. Chem. Lett*. **2006**, 16(17), 4633-4637. https://doi.org/10.1016/j.bmcl.2006.06.012
38. Manosuthi, W.; Wiboonchutikul, S; Sungkanuparph, S. Integrated therapy for HIV and tuberculosis. A*IDS Res. Ther*. **2016**, 13:22. https://doi.org/10.1186/s12981-016-0106-y
39. Khan, S.A.; Akthar, M.J.; Gogoi, U.; Meenakshi, D.U.; Das, A. An overview of 1,2,3-triazole-containing hybrids and their potential anticholinesterase activities. *Pharmaceuticals*, **2023**, 16(2): 179. https://doi.org/10.3390/ph16020179
40. Eswaran, S.; Adhikari, A.V.; Shetty, N.S. Synthesis and antimicrobial activities of novel quinoline derivatives carrying 1,2,4-triazole moiety. *Eur. J. Med. Chem*. **2009**, 44(11), 4637-4647. https://doi.org/10.1016/j.ejmech.2009.06.031
41. Casano, G.; Dumétre, A.; Panneouque, C.; Hutter, S.; Azas, N.; Robin, M. Anti-HIV and antiplasmodial activity of original flavonoid derivatives. *Bioorg. Med. Chem*. **2010**, 18 (16), 6012-6023. https://doi.org/10.1016/j.bmc.2010.06.067
42. Indrayanto, G., Putra, G.S.; Suhud, F. Chapter Six - Validation of in-vitro bioassay methods: Application in herbal drug research, in Profiles of Drug Substances, Excipients and Related Methodology, A.A. Al-Majed, Editor. *Profiles Drug Subst. Excip. Relat. Methodol*. **2021**, 46, 273-307. https://doi.org/10.1016/bs.podrm.2020.07.005
43. Kumar, S.; Mehra, R.; Sharma, S., Bokolia, N.P.; Raina, D.; Nargotra, A.; Singh, P.P.; Khan, I.A. Screening of antitubercular compound library identifies novel ATP synthase inhibitors of Mycobacterium tuberculosis. *Tuberculosis*, **2018**, 108, 56-63. https://doi.org/10.1016/j.tube.2017.10.008
44. El-Zohairy, M.A.; Zlotos, D.P.; Berger, M.R.; Adwan, H.H.; Mandour, Y.M. Discovery of Novel CCR5 Ligands as anticolorectal cancer agents by sequential virtual screening. *ACS Omega*, **2021**, 6 (16), 10921-10935. https://doi.org/10.1021/acsomega.1c00681
45. Vadivelu, A.; Gopal, V.; Reddy, C.U.M. Molecular docking studies of 1, 3, 4-thiadiazoles as novel peptide deformylase inhibitors as potential antibacterial agents. *Int. J. Pharm. Sci. Rev. Res*. **2015**, 31(1) 58-62.

 doi:10.20944/preprints202504.0967.v1

https://citeseerx.ist.psu.edu/document?repid=rep1&type=pdf&doi=327843d2a59588c3263726dc53a4b9d2f04c519f

46. Shah, P.; Naik. D.; Jariwala, N.; Bhadane, D.; Kumar, S.; Kulkarni, S.; Bhutani, K.K.; Singh, I.P. Synthesis of C-2 and C-3 substituted quinolines and their evaluation as anti-HIV-1 agents. *Bioorg. Chem*. **2018**, 80, 591-601. https://doi.org/10.1016/j.bioorg.2018.07.016
47. Ibrahim, T.S.; Bokhtia, R.; Al-Mahmoudy, A.M.M.; Taher, E.S.; AlAwadh, M.A.; Elagawany, M.; Abdel-Aal, E.H.; Panda, S.; Gouda, A.M.; Asfour, H.Z.; Alhakamy, N.A.; Youssif, B.G.M. Design, synthesis and biological evaluation of novel 5-((substituted quinolin-3-yl/1-naphthyl) methylene)-3-substituted imidazolidin-2,4-dione as HIV-1 fusion inhibitors. *Bioorg. Chem*. **2020**, 99,103782. https://doi.org/10.1016/j.bioorg.2020.103782
48. Oyeneyin, O.E.; Ojo, N.D.; Ipinlogu, N.; James, A.C.; Agbaffa, E.B. Investigation of corrosion inhibition potentials of some aminopyridine Schiff bases using density functional theory and Monte Carlo simulation. *Chem. Afr*. **2022**, 5, 319-322. https://doi.org/10.1007/s42250-021-00304-1
49. Zhan, C.-G.; Nichols, J.A.; Dixon, D.A. Ionization potential, electron affinity, electronegativity, dardness, and electron excitation energy: Molecular properties from density functional theory orbital energies. *J. Phys. Chem. A*, **2003**, 107(20). 4184-4195. https://doi.org/10.1021/jp0225774
50. Kadi, I.; Güldeniz, S.; Bouled, H.; Zebbiche, Z.; Suat, T.; Fatümetüzzehra, K.; Gönül, Z.; Küçükbay, H.; Boumoud, T. Synthesis, cytotoxicity, antioxidant activity, DFT calculations, and docking studies of new pyridine-malonate derivatives as potential anticancer agents. *Polycycl. Aromat. Compd*. **2022**, 44(10), 6615-6629. https://doi.org/10.1080/10406638.2023.2281468
51. Hussain, Z.; Ibrahim, M.A.; Hassanin, N.M.; Badran, A-S. Synthetic approaches for novel annulated pyrido[2,3-d]pyrimidines: Design, structural sharacterization, Fukui functions, DFT calculations, molecular docking and anticancer efficiency. *J. Mol. Struct*. **2024**, 1318(1), 139335. https://doi.org/10.1016/j.molstruc.2024.139335
52. Roskoski Jr, R. Properties of FDA-approved small molecule protein kinase inhibitors. *Pharmacol. Res.* **2024**, 200: 107059. https://doi.org/10.1016/j.phrs.2024.107059
53. Wei, X.; Decker, M.J.; Liu, H.; Zhang, Z.; Arani, R.B.; Kilny, J.M.; Saag, M.S.; Wu, X.; Shaw, G.M.; Kappes, J.C. Emergence of resistant human immunodeficiency virus type 1 in patients receiving fusion inhibitor (T-20) monotherapy. *Antimicrob. Agents Chemother*. **2002**, 46(6), 1896-1905. https://doi.org/10.1128/AAC.46.6.1896-1905.2002
54. Naidu, D.; Oduro-Kwateng, E.; Solima, M.E.S.; Ndlovu, S.I.; Mkhwanazi, N.P. Alternaria alternata (Fr) Keissl crude extract inhibits HIV subtypes and integrase drug-resistant strains at different stages of HIV replication. *Pharmaceuticals*, **2025**, 18(2), 189. https://doi.org/10.3390/ph18020189
55. Sastry, M.G.; Adzhigirey, M.; Day, T.; Annabhimoju, R.; Sherman, W. Protein and ligand preparation: parameters, protocols, and influence on virtual screening enrichments. *J. Comput. Aided Mol. Des*. **2013**, 27(3), 221-234. https://doi.org/10.1007/s10822-013-9644-8
56. Mohammadpourasl, S.; de Biani, F.F.; Coppola, C.C.; Parisi, M.L.; Zani, L.; Dessi, A.; Calamante, M.; Reginato, G.; Basosi, R.; Sinicropi, A. Ground-State redox potentials calculations of D-π-A and D-A-π-A organic dyes for DSSC and visible-light-driven hydrogen production. *Energies*, **2020**, 13(8) 2032. https://doi.org/10.3390/en13082032
57. Aslam, R., Serdaoglu, G.; Zehra, S.; Verma, K.D.; Aslam, J.; Guo, L.; Verma, C.; Ebenzo, E.E.; Quraishi, M.A. Corrosion inhibition of steel using different families of organic compounds: Past and present progress. *J. Mol. Liq*. **2022**, 348, 118373. https://doi.org/10.1016/j.molliq.2021.118373
58. Ibrahim, M.A., Roushdy, N.; Atta, A.A.; Badran. A-S.; Farag, A.A.M. Comprehensive study on pyrano[3,2-c]quinoline-based indole: Synthesis, characterization, and potential for optoelectronic and photovoltaic applications. *J. Mol. Struct*. **2024**, 1312, 138660. https://doi.org/10.1016/j.molstruc.2024.138660

 doi:10.20944/preprints202504.0967.v1

disclaim responsibility for any injury to people or property resulting from any ideas, methods, instructions or products referred to in the content.